# Measuring Close Binary Stars with Speckle Interferometry

**Keith T. Knox**
*Air Force Research Laboratory*

## ABSTRACT

Speckle interferometry (Labeyrie, 1970) is a well-tested and still used method for detecting and measuring binary stars that are closer together than the width of the atmospheric seeing disk. In this method, an average spatial power spectrum is computed from a series of short-exposure images. The power spectrum exhibits clearly defined cosine fringes, while the autocorrelation function (its Fourier Transform) contains a central peak with two side lobes. Over the years, several methods have been developed to analyze either the autocorrelation function or the power spectrum to determine the separation and orientation of the binary star system (Horch, 1996, Tokovinin, 2010).

In this talk, a method for analyzing the fringes in the power spectrum will be described to robustly detect and measure the fringes. The method is based on the detection of the fringe minima and the inflection points between the minima and the maxima. An analysis of the effects of working with the uncalibrated (or poorly calibrated) power spectrum was done. It was found that this method provides a robust detection of the presence of fringes, but that the estimation of the separation of the binary star system has a systematic bias towards larger values. This bias can be overcome with a subsequent inspection of the fringes.

## 1. INTRODUCTION

The study of binary star systems, i.e. stars that orbit each other, has many practical uses, besides the obvious astronomical ones. By observing binary stars with known separations, one can calibrate an imaging system in terms of its resolution and its plate scale, i.e. the angular field-of-view of an individual pixel.

Very close binary stars, i.e. stars whose angular separation is smaller than the blur size of the atmospheric turbulence seeing disk, require extra effort to be measured. One method of observing such binary star systems is to use adaptive optics to correct the atmospheric blur in real-time, resulting in direct images of the binary pair. A recent example of this application can be found in an article by Jack Drummond [1].

Not every telescope has access to an adaptive optics system, and those telescopes utilize a prior method developed in 1970 by Antoine Labeyrie [2]. This method, called speckle interferometry, consists of capturing many short-exposure images of the binary star system and averaging the power spectrum to recover the separation and orientation of the binary star system. Because the exposure time is short enough to freeze the motion of the atmospheric turbulence, the binary star takes on a speckled appearance. The presence of two stars within the image gives rise to fringes in the power spectrum. The presence and analysis of the fringes derived from the speckle images gives rise to the name “speckle interferometry.”

In this paper, a method for detecting and analyzing binary stars from the fringes produced by speckle interferometry is proposed. The goal of the proposed method is to increase the likelihood of detection of the fringes and to develop a method that can be automated. A series of short exposure images of three close visual binaries was obtained from Dr. Russell Genet of California Polytechnic State University, Cuesta College and the University of North Dakota. These images are used to demonstrate the proposed method.

## 2. DATA COLLECTION

In October 2013, Russell Genet gathered speckle images of several binary star systems [3]. The data analyzed in this paper was taken on the 2.1-meter telescope at Kitt Peak, shown in Fig. 1. Three example image sets from this observing run were provided on three stars, namely WDS 01017+2518, WDS 21399+2737 and WDS 23019+4220. All of these binary stars have published separations that are very close to, or even less than, the diffraction limit of the 2.1-meter telescope.

Fig. 1. Russell Genet standing next to the 2.1-meter telescope at Kitt Peak Observatory.

For each star, a thousand frames were taken with 10 msec exposure times. An i' filter was used, which has a geometric mean of 770 nm. The focal plane array contained 512 x 512 pixels, with an instantaneous FOV equal to 0.0117 "/pixel. For the 2.1-meter telescope at 770 nm, the resolution half angle, 1.22 λ/D, is equal to 0.092".

Example speckle images of the three binary stars are shown in Fig. 2. The binary on the left, WDS 01017+2518, has a published separation of 0.074". It is a pair of stars that have almost the same brightness, 7.75 $m_v$ and 7.5 $m_v$. The binary in the middle of Fig. 2, WDS 21399+2737, has a magnitude difference of one, 11.95 $m_v$ and 13.2 $m_v$, with a published separation of 0.154". The third binary on the right, WDS 23019+4220, has a published separation of 0.191" and an even larger magnitude difference, 3.7 $m_v$ and 6.0 $m_v$.

Because the stars in WDS 23019+4220 are so bright, the speckles in the short-exposure image are well formed. The middle binary in Fig. 2, WDS 21399+2737, on the other hand, is so dim that speckles are not apparent in the image. As will be seen in the following analysis, the larger the magnitude difference between the binary pair, the more difficult it is to detect the presence of the binary in the speckle interferometry fringes.

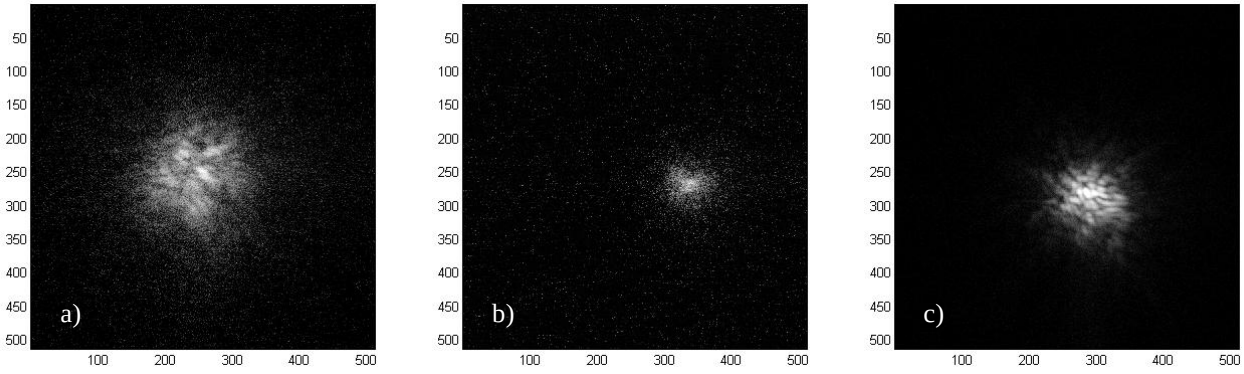


Fig. 2. Single images of three binary stars, a) WDS 01017+2518, b) WDS 21399+2737 and c) WDS 23019+4220.

## 3. SPECKLE INTERFEROMETRY

In 1970, Antoine Labeyrie [2] developed a technique to detect double stars that are closer than the width of the atmospheric seeing disk. This method is routinely used today to measure the separation of double or binary stars that are closer together than an angular separation of 1 arc second. The method consists of computing the Fourier transform of each image frame, taking the square modulus, and adding the transforms together. The resultant sum contains straight line "cosine" fringes that indicate the separation and orientation of the two objects.

This method is based on the concept that two objects that are very close together, when viewed through the atmosphere, are blurred by the exact same atmospheric point spread function. If both of the objects are unresolved, then the image consists of the exact same atmospheric point spread function placed at two locations in the frame and summed together. Although Labeyrie's method was devised for objects that are closer together than the width of the atmospheric point spread function, it works for objects that are farther apart, as long as the two objects are in the same isoplanatic patch, i.e. the same atmospheric point spread function is applied to both objects.

If the atmospheric point spread function is p(x, y), then the image of the two objects is given by:

$$i(x,y) = p\left(x - \Delta x/2, y - \Delta y/2\right) + ap\left(x + \Delta x/2, y + \Delta y/2\right), \tag{1}$$

where, *a*, is the brightness ratio of the two objects, and the separation distance between them, *d*, is given by:

$$d = \sqrt{\Delta x^2 + \Delta y^2}\ . \tag{2}$$

The Fourier transform of the image, *I*, converts the translation shifts, $\Delta x$ and $\Delta y$, into linear phase factors. Capital letters are used to represent the Fourier transform of the corresponding quantity.

$$I(u,v) = P(u,v)\left(e^{-i(\Delta xu + \Delta yv)/2} + ae^{i(\Delta xu + \Delta yv)/2}\right) \tag{3}$$

The square modulus of the Fourier transform of the image, *I*, becomes:

$$\left|I(u,v)\right|^2 = \left|P(u,v)\right|^2\left[(1-a)^2 + 4a\cos^2\left(\Delta xu/2 + \Delta yv/2\right)\right] \tag{4}$$

If the two objects are the same brightness, i.e. $a = 1$, then the square modulus is:

$$\left|I(u,v)\right|^2 = \left|P(u,v)\right|^2 4\cos^2\left(\Delta xu/2 + \Delta yv/2\right) \tag{5}$$

This equation shows that the square modulus of the Fourier transform is the product of the square modulus of the Fourier transform of the point spread function, and a set of cosine-squared fringes, whose separation and orientation depend inversely on the separations, $\Delta x$ and $\Delta y$, in the image. Any arbitrary random shift, due to the random motion of the atmospheric turbulence, is removed in the power spectrum, eliminating any need for re-centering.

In Fig. 3 are shown an example image from WDS 01017+2518 and the result of summing the power spectra from 1,000 individual frames. The contrast of the average power spectrum in 3 b) has been stretched by taking the logarithm of the spectrum to enhance to low contrast information.

In the power spectrum in Fig. 3 b), two dark lines are clearly visible on either side of the central peak. The circular shape within the power spectrum corresponds to the extent of the diffraction limit. Note that in this case, the dark fringe lines (minima of the cosine) are within the diffraction limit. The orientation of the two binary stars is in the direction perpendicular to the orientation of the dark lines themselves.

For this case, where the two stars are approximately the same brightness, the brightness ratio, *a*, in equation (4) is approximately unity, resulting in a simple product of cosine squared with no additive constant. The effects of a non-zero additive constant will become apparent in section 5.

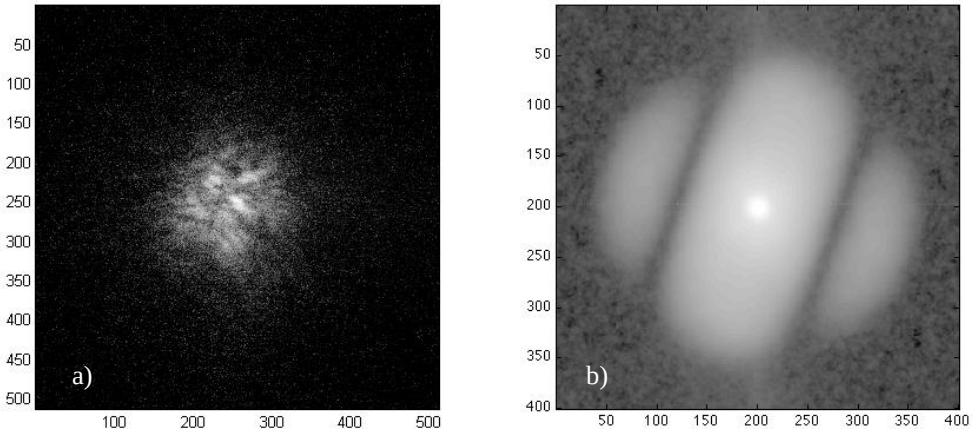


Fig. 3. Image of the double star, WDS 01017+2518, a) single frame, b) the sum of 1,000 power spectra. Each power spectrum is the square modulus of the Fourier transform of the individual short-exposure frame.

## 4. RAYLEIGH CRITERION

A common description of the resolution of a telescope is the Rayleigh criterion. This criterion is based on the theoretical diffraction limit of the telescope, which is illustrated in Fig. 4. The point spread function (PSF) of the telescope, also called the Airy Disk, is shown in Fig. 4 a), with a cross-section through the middle shown in 4 b). The half angle of the center lobe of the Airy Disk is the angular distance between the maximum at zero frequency and the first zero at 1.22λ/D, where λ is the wavelength of the light and D is the diameter of the telescope. As seen in Fig. 4 c), the highest spatial frequency that can get through the telescope and into the image is given by D/λ.

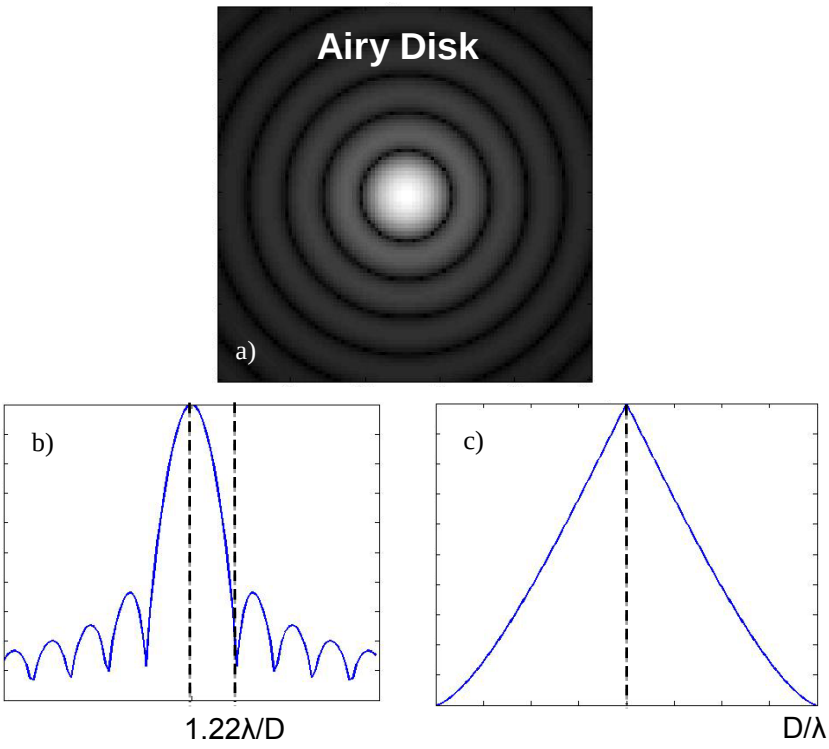


Fig. 4. The Airy disk is the theoretical response of the telescope to a point source, or the point spread function, in the absence of atmospheric turbulence. Shown in this figure are a) an image of the Airy Disk, b) the cross-section of the Airy Disk, showing the first zero occurring 1.22λ/D away from the center peak, where λ is the wavelength and D is the diameter of the telescope, and c) a cross-section of the power spectrum, showing a cutoff at a frequency of D/λ.

The Rayleigh Criterion says that the smallest distance between two point objects at which they can be seen as distinct objects is the half angle of the Airy Disk. An image of two objects separated by that distance is illustrated in Fig. 5 a). The Fourier transform of the image of those two objects is shown in 5 b).

There are three important points to note from this illustration. The first is that the Fourier transform of the image of the two objects exhibits the dark lines of the minima of the cosine-squared function from equation (5). The second point is that the dark lines corresponding to the minima of the cosine are oriented perpendicularly to a line drawn between the two objects in Fig. 5 a). The third point (and most important one) to note from this figure is that the first minimum/zero of the cosine-squared function occurs well within the diffraction limit of the telescope.

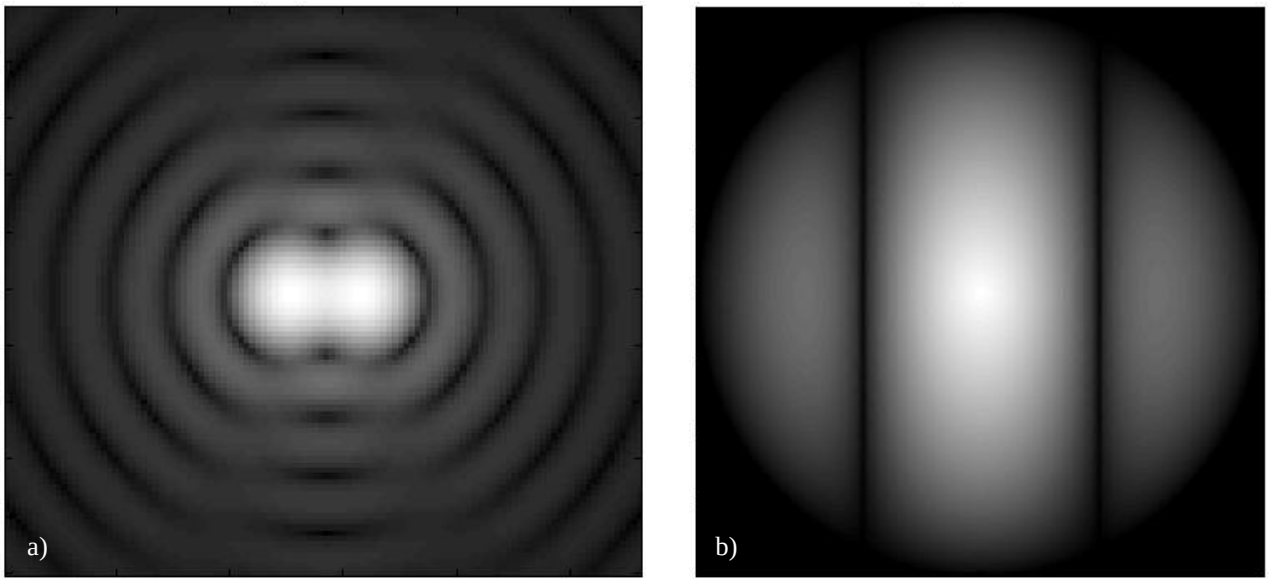


Fig. 5. An image of two point sources separated by the amount corresponding to the Rayleigh criterion, i.e. a separation equal to the half-angle of the Airy Disk (1.22λ/D). Shown in this figure are a) the two point sources, and b) the Fourier transform of the image in a). The visible fringe in b) results from the two identical sources in a).

The location of the first minimum in the cosine-squared function is given where the argument of the cosine function is equal to π/2. For simplicity, and with no loss in generalization, this analysis will be reduced to one dimension. From equation (4), it can be seen that the frequency ($u/2\pi$) where the cosine is zero is given by:

$$\frac{u\Delta x}{2} = \frac{\pi}{2}, \text{ or}$$
$$u/2\pi = \frac{1}{2}\frac{1}{\Delta x} \tag{6}$$

If the separation of the two objects, Δx, is given by the Rayleigh Criterion ($1.22\lambda D$), then the first minimum is located at:

$$u/2\pi = \frac{1}{2.44}\frac{D}{\lambda} \tag{7}$$

In other words, the first minimum (dark line) is located less than halfway out to the diffraction limit cutoff, $D/\lambda$. That says that separations less than the Rayleigh Criterion are detectable if the location of the first minimum can still be determined. Clearly, if the first minimum occurs before $D/\lambda$, then it has a good chance of being detected. This question is discussed by Elliott Horch [4], where he proposes fitting an asymmetric PSF is used to determine the location of the first minimum.

## 5. EFFECTS OF ATMOSPHERIC PSF

The cosine-squared fringes from equation (4) are modified by the Optical Transfer Function (OTF) of the atmosphere, which is the Fourier transform of the atmospheric point-spread function (PSF). This OTF is a combination of the Fourier transform of the Airy Disk, see Fig. 4 c), and the effects of the atmospheric turbulence.

It is common [3, 5, 6] to measure nearby isolated single stars to gain a measure of the power spectrum (OTF squared) of the atmosphere. This power spectrum is then divided into the power spectrum of the binary star to mitigate the effects of the degradation of the binary power spectrum by the atmosphere.

The effect of the atmospheric PSF/OTF is illustrated in Fig. 6. The cosine-squared fringes are shown in 6 a) overlaid on top of a Gaussian function, which represents a generic atmospheric OTF. Note that the cosine-squared fringes do not go to zero at the minima, but instead are offset by a constant equal to $(1\text{-}a)^2$, where, $a$, is relative brightness ratio of the two stars. When the two stars are of equal brightness, then there is no offset constant.

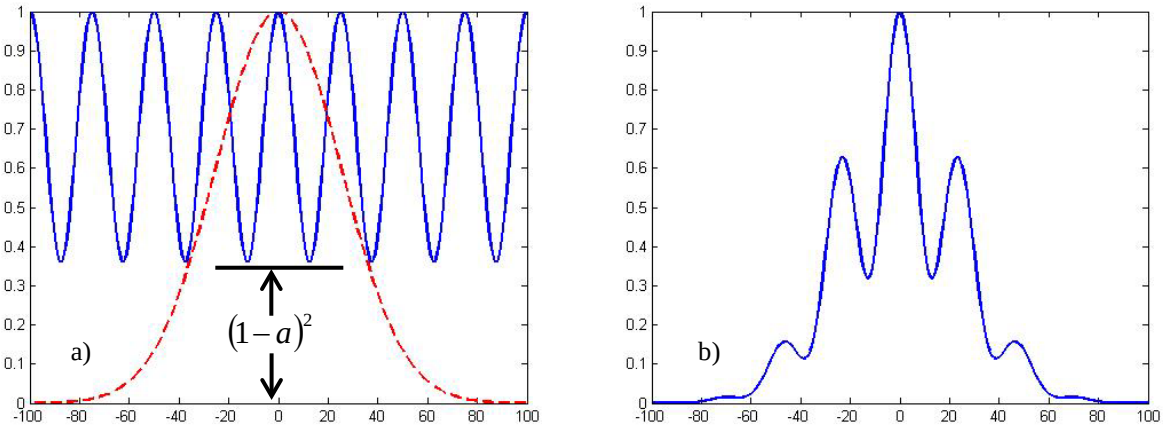


Fig. 6. The cosine fringes (solid line) are shown on the left, a), drawn on top of an atmospheric PSF (dashed line). On the right, b), is shown the product of the PSF with the cosine fringes.

The product of the fringes with the atmospheric OTF is shown in Fig. 6 b). From a simple glance at this figure, it would appear the values of the maxima and minima are changed, but their locations are otherwise left alone.

In Fig. 7, the cosine fringes are compared to modified fringes. Vertical lines are drawn at the locations of one minimum and one maximum. By sighting along these lines, it can be seen that the maxima and minima shift with respect to the center of the OTF. The maxima can be seen to move inward towards the center of the OTF, while the minima move outwards. The amount of movement depends on the value of the constant offset, which is a function of the relative brightness of the two objects.

Although not illustrated in this figure, it can be shown that the inflection points between the minima and maxima also move inward with the maxima.

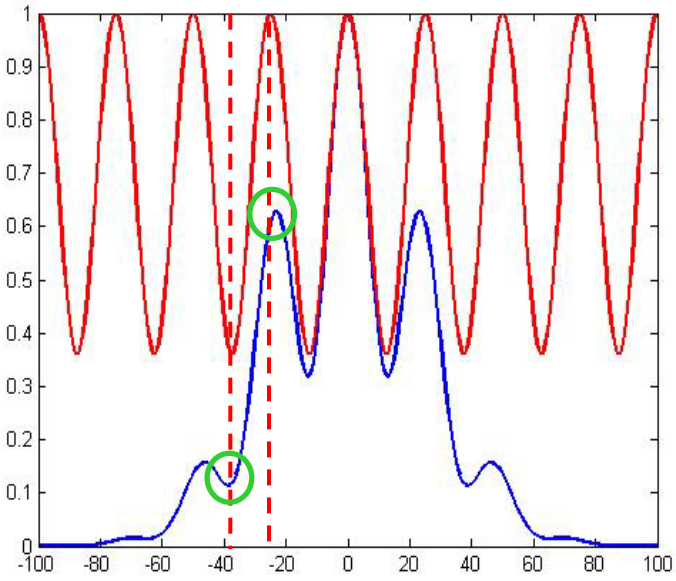

Fig. 7. Cosine fringes are drawn with the product of the atmospheric PSF and the cosine fringes. Vertical dashed lines show that the maxima in the cosine fringes move inward towards the center, while the minima move outward.

## 6. DETECTING FRINGES

The fringe separation can be measured by determining the distance between adjacent minima or between adjacent maxima. Theoretically, one could use either distance to measure the fringe separation. From the previous section, though, the maxima appear to be more sensitive to movement by the multiplication of the atmospheric OTF than are the minima. In fact, when the two objects have equal brightness, the minima are exactly zero and the locations of the minima do not move at all. Even in this case, though, the maxima still move inward. As a result, the determination of the fringe separation from the minima is less sensitive to the effects of the atmospheric OTF than from the maxima.

The location of the minima and maxima are given by the locations where the first derivative of the power spectrum goes to zero. This is not easy, though, because the region where the first derivative goes to zero is very thin line. To determine whether the zero region is a minimum or a maximum, the second derivative needs to be inspected. If the second derivative is greater than zero, then it is a minimum.

While inspecting the second derivative, it was discovered that the region of positive second derivative (indicating a minimum) was much broader than the region of zero first derivative and therefore easier to detect. This region is the space between the two inflection points, in between where the second derivative goes to zero.

Since the fringes can be oriented in an arbitrary direction, the second derivatives in the horizontal, vertical and diagonal directions are combined together to find the maximum variation. As the second derivative of the fringes is periodic, the autocorrelation of the second derivative is also periodic. The autocorrelation of the two-dimensional second derivative is shown in Fig. 8. A result of computing the autocorrelation is that the resultant fringes are significantly smoothed without changing the periodicity, making it easier to detect the fringe spacing.

Minima and maxima are defined by the locations where the first derivatives are zero.

$$\left(\frac{\partial}{\partial x}\right)^2 + \left(\frac{\partial}{\partial y}\right)^2 = 0$$

The region containing the minima is where the second derivatives are greater than zero.

$$\frac{\partial^2}{\partial x^2} > 0, \frac{\partial^2}{\partial y^2} > 0$$

The two-dimensional autocorrelation of the second derivative of the fringes produces a duplicate set of fringes.

$$\text{Autocorrelation} = \frac{\partial^2}{\partial x^2} \otimes \frac{\partial^2}{\partial x^2}$$

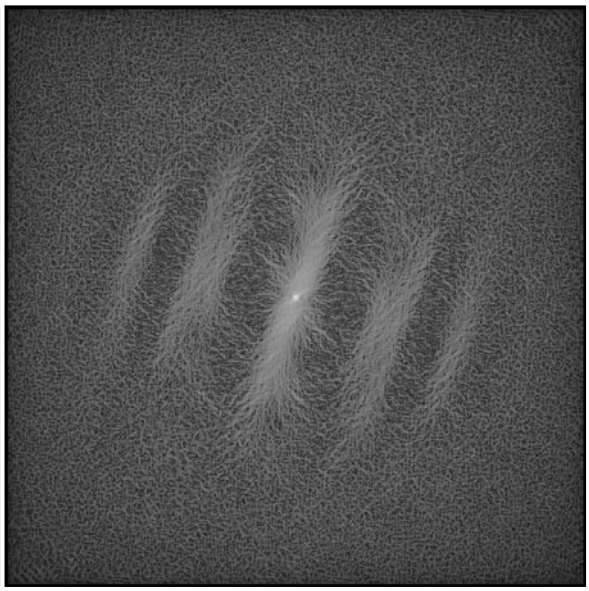

Fig. 8. The two-dimensional autocorrelation of the second derivative of the fringes of binary star, WDS 0107+2518.

Once the fringes are revealed in the second derivative, they need to be detected. This is accomplished through integration at different angles. In a Hough Transform-like operation, integration along parallel lines oriented at many different angles is computed. This is illustrated in Fig. 9. The left side of the figure shows the original power spectrum fringes, while the right side shows the corresponding autocorrelation of the second derivative.

The yellow lines in Fig 9 b) illustrate the integration for one angle. The integration along the parallel lines produces a one-dimensional function with potential peaks and valleys. When the direction of integration is aligned with the fringes, the peak and valleys will have the maximum excursions, or maximum modulation. The modulation is

defined as the difference in values between an adjacent peak and valley, divided by their sum. When the direction of integration is perpendicular to the fringes, the peaks and valleys will disappear and the modulation will go to zero.

The integration of the second derivative when the direction of integration is in alignment with the fringes is shown in Fig. 10 a). Since the result of this integration is so noisy, the autocorrelation of the integration, shown in Fig. 10 b), is computed to make the determination of the locations of the peaks and valleys easier.

For each angle of orientation of the integration, the modulation of the resultant fringes is computed. A plot of this modulation is shown in Fig. 11. When the integration is aligned with the fringes, the modulation is a maximum. From this plot, the direction of the fringes can be determined.

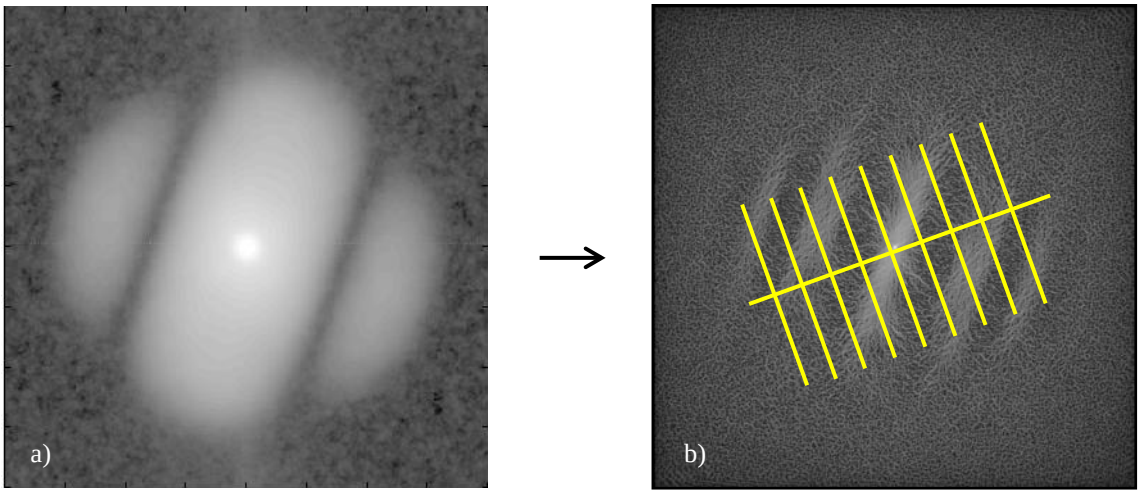


Fig. 9. The fringes from WDS 01017+2518, a), are converted to the autocorrelation of the second derivative, b). This derivative function is integrated along parallel lines (shown in yellow) oriented at several different angles, in a Hough Transform-like operation.

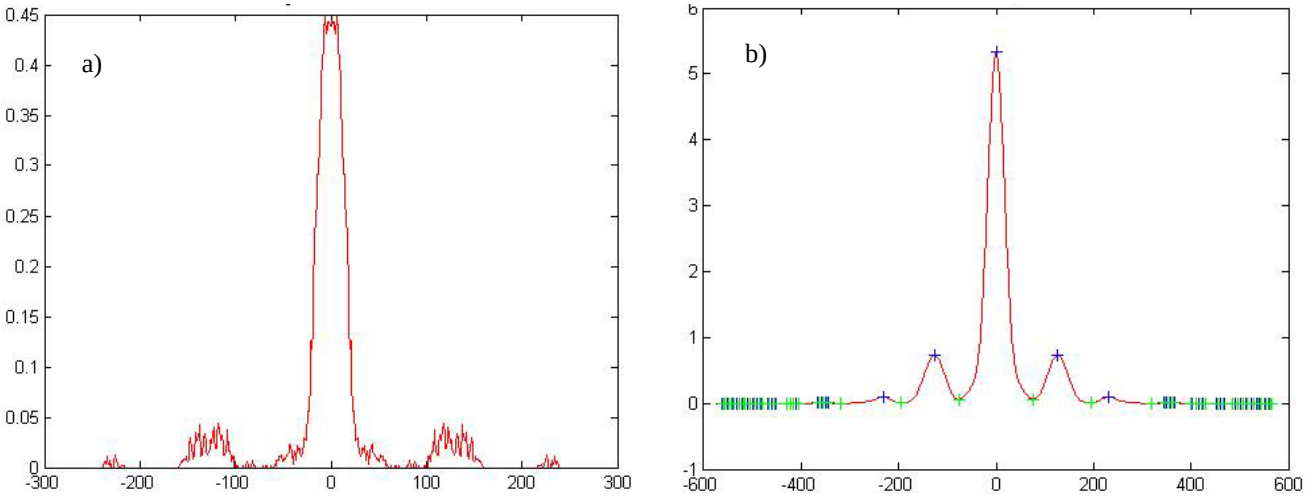


Fig. 10. The integration of the second derivative at an example angle is shown in a). The one-dimensional autocorrelation of this function is shown in b). The distance between the center peak and the first side peak is equal to the fringe separation in Fig. 9 a).

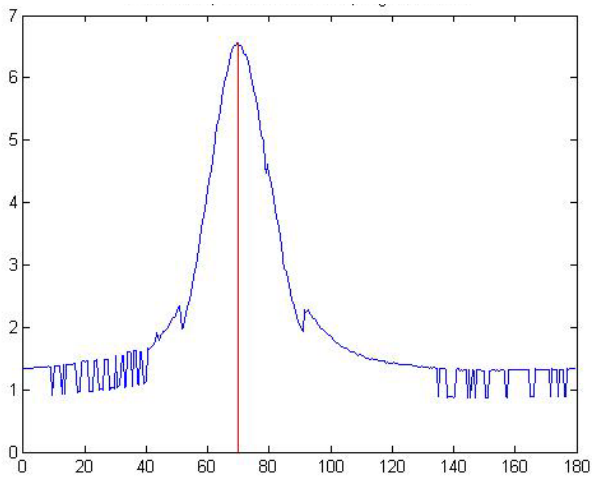


Fig. 11. The integration shown in Fig 10 b) is computed at several orientations. This figure shows the plot of the modulation of the computations. The example shown in Fig. 10 was computed at the angle of the peak modulation.

## 7. RESULTS

The results of this method, applied to the data from the three binary stars, are shown below in Fig. 12. The raw power spectra show fringes to the eye to varying degrees, depending on the magnitude difference of the binary stars. In the bottom row, though, the detected fringes are more evident, and even indicate some surprises.

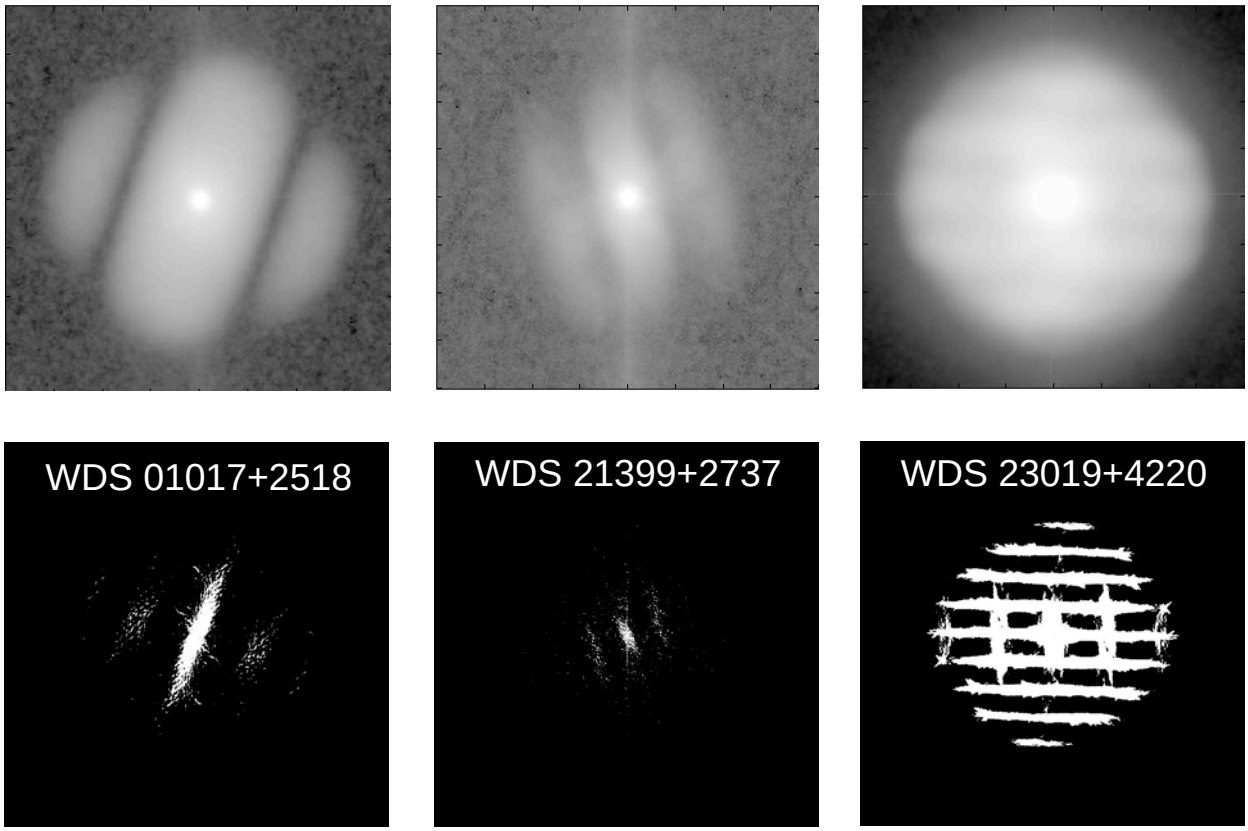


Fig. 12. The power spectra for the three binary stars are shown in the top row. In the bottom row are thresholded versions of the computed autocorrelations of the second derivatives, yielding detected fringes.

The fringes for the two stars on the left side of Fig. 12 appear as expected. The fringes are visible in the raw power spectra and they have been detected in the thresholded second derivatives. The fringes for WDS 23019+4220, though, are very different. In the raw spectrum, the fringes are hard to see. This is not unexpected, since the magnitude different for this binary is slightly greater than 2. Even so, the power spectrum appears muddled

In the detected fringes for WDS 23019+4220, the expected fringes are detected, but there appear to be a second set of fringes in a perpendicular direction. Referring back to the raw power spectrum, it is possible to imagine a faint set of potential fringes in that direction. The modulation computation sees the clear horizontal fringes, but does not pick up the smaller perpendicular fringes apparent in Fig. 12. This star is reported to be a double-double star, but this result cannot claim to confirm that conclusion.

The fringe separations, computed from the fringe detections in Fig. 12, are shown in Fig. 13, plotted on top of the raw power spectra. By visual inspection, there is a systematic underestimation of the fringe spacing. This is not surprising, since as mentioned in section 5, the effect of the uncorrected atmospheric OTF is to move the inflection points (the zeroes of the second derivative) inward towards the center. That is exactly what is observed in Fig. 13.

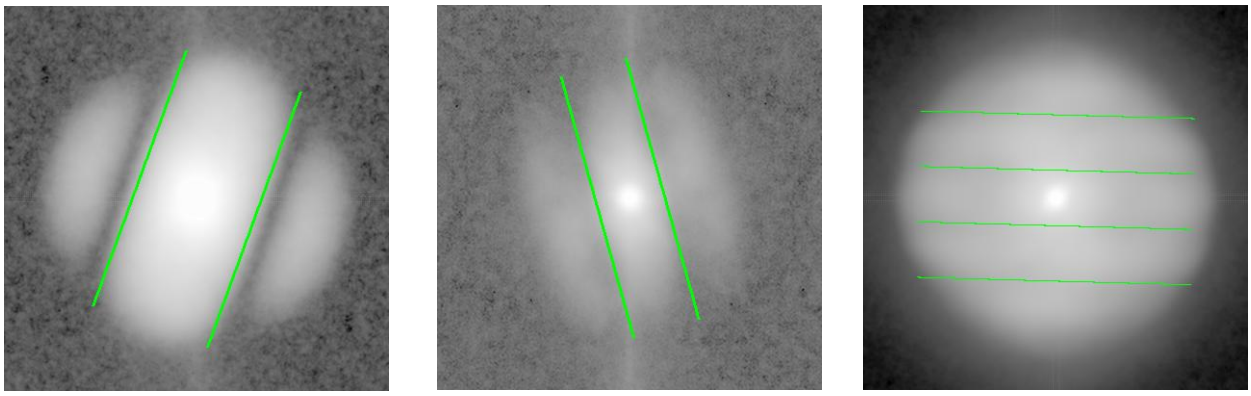

Fig. 13. The computed fringe separations are shown plotted in green on top of the raw power spectra.

Having determined the orientation of the fringes and the approximate location of the fringe minima, a localized search was made in the raw power spectra for the minimum integrated value along the fringe lines. The result of that search is shown in Fig. 14. By visual inspection, the new fringe locations appear to be correct. The separations computed from these fringe spacings are compared with published values in Table 1, below.

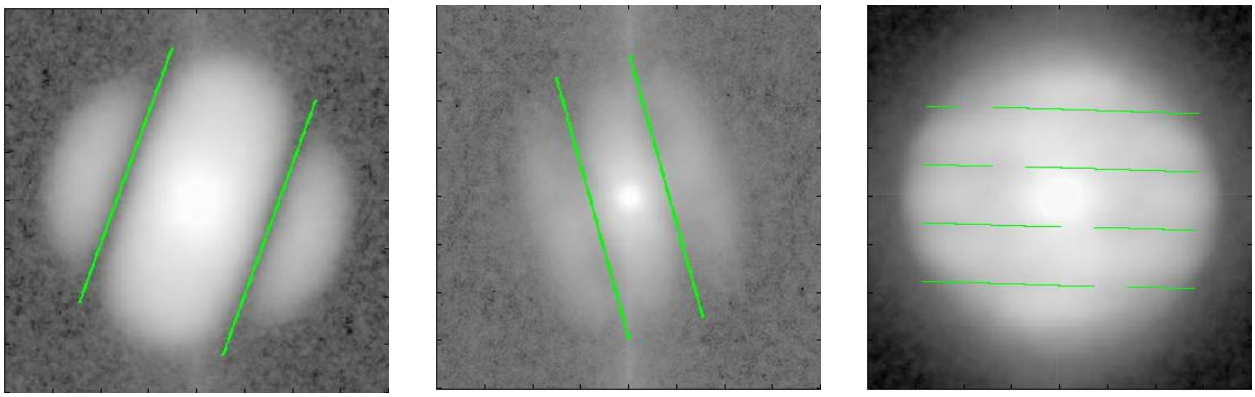

Fig. 14. Recomputed fringe separations, found by searching for the minimum values in the detected orientation.

| | Measured | Published |
|---|---|---|
| WDS 01017+2518 | 0.075” | 0.074” |
| WDS 21399+2737 | 0.150” | 0.154” |
| WDS 23019+4220 | 0.196” | 0.191” |

Table 1

## 8. CONCLUSIONS

A method was proposed to detect fringes in speckle interferometry imagery using the inflection points in the second derivative of the power spectra. It has been shown that this method is able to detect fringes that are barely visible to the eye. It was also shown that these estimates of the separation of the binary pair are systematically too large, due to the displacement of the minima of the fringes by the atmospheric OTF, when left uncorrected. Even so, these estimates give a good indication of the orientation of the fringes and a reasonable enough value of the fringe spacing, to allow a localized search of the raw power spectrum to determine a more accurate measurement of the fringe spacing. Although this method produces a slightly biased value for the separation, it is good enough to confirm detection of the presence of fringes and to give a good initial value for a more detailed automatic search for the true minimum value. In comparison with the published values, the computed separations of the three stars are very close for each binary.

## 9. REFERENCES


1. Drummond, J. D., "Binary Stars Observed with Adaptive Optics at the Starfire Optical Range", *The Astronomical Journal*, vol. 147, No. 3, pp. 65-74 (2014).
2. Labeyrie, A, "Attainment of diffraction limited resolution in large telescopes by Fourier analysing speckle patterns in star images", Astronomy and Astrophysics, vol. 6, p. 85, (1970).
3. Genet, R. M., et al, "Kitt Peak Speckle Interferometry of Close Visual Binary Stars", Proc. 33rd Annual Symposium On Telescope Science, Eds. Brian D. Warner, Robert K. Buchheim, Jerry L. Foot, and Dale Mais., pp. 77-91, (2014).
4. Horch, E.P., "Characterizing Binary Stars Below the Diffraction Limit with CCD-Based Speckle Imaging", *Astronomical Journal*, **132**, pp. 2478-2488, (2006).
5. Horch, E. P., et al, "Speckle Interferometry of Southern Double Stars", *Astronomical Journal.*, **111**, pp. 1681-1688, (1996).
6. Tokovinin A., et al, "Speckle Interferometry at the Blanco and SOAR Telescope in 2008 and 2009", *Astronomical Journal*, **139**, pp. 743-756, (2010).